AIP | Review of Scientific Instruments

Narrow band wavelength selective filter using grating assisted single ring resonator

P. Prabhathan and V. M. Murukeshan

Citation: Review of Scientific Instruments **85**, 093111 (2014); doi: 10.1063/1.4896040
View online: http://dx.doi.org/10.1063/1.4896040
View Table of Contents: http://scitation.aip.org/content/aip/journal/rsi/85/9?ver=pdfcov
Published by the AIP Publishing

Narrow band wavelength selective filter using grating assisted single ring resonator

P. Prabhathan[a] and V. M. Murukeshan
Centre for Optical & Laser Engineering (COLE), School of Mechanical and Aerospace Engineering, Nanyang Technological University, 50 Nanyang Avenue, Singapore 639798

(Received 10 June 2014; accepted 6 September 2014; published online 24 September 2014)

This paper illustrates a filter configuration which uses a single ring resonator of larger radius connected to a grating resonator at its drop port to achieve single wavelength selectivity and switching property with spectral features suitable for on-chip wavelength selection applications. The proposed configuration is expected to find applications in silicon photonics devices such as, on-chip external cavity lasers and multi analytic label-free biosensors. The grating resonator has been designed for a high Q-factor, high transmittivity, and minimum loss so that the wavelength selectivity of the device is improved. The proof-of-concept device has been demonstrated on a Silicon-on-Insulator (SOI) platform through electron beam lithography and Reactive Ion Etching (RIE) process. The transmission spectrum shows narrow band single wavelength selection and switching property with a high Free Spectral Range (FSR) ~60 nm and side band rejection ratio >15 dB © *2014 AIP Publishing LLC*. [http://dx.doi.org/10.1063/1.4896040]

I. INTRODUCTION

Photonic Integrated Circuits(PIC) would enable creation of multifunctional optical devices with unique capability of high efficiency, compactness, and mass fabrication possibilities.[1] Wavelength filters are one of the critical components in a PIC design since they can find applications ranging from optical signal processing [2–4] to bio-sensing.[5–7] A ring resonator with its unique property of compactness and simplicity is highly suitable for on-chip wavelength filtering functionality.[8] However, for a ring resonator the spectral response is periodic in nature and supports large number of resonances with separation between them given by the Free Spectral Range (FSR). Generally two methods have been applied to increase the FSR of a ring resonator so that a single wavelength selection is possible over a wide FSR. First one is to reduce the radius of the ring.[9] But the extremely small radius will cause high bending loss and radiation loss in the structure along with the fabrication challenges in achieving this small dimension. The second approach involves creating Vernier configuration of multiple ring resonators.[10,11] However, in a Vernier configuration, the high FSR is achieved through resonance mismatch among two ring resonators which would causes presence of side modes in the output spectrum. For spectral response shaping in such devices, control of the couplings between the micro rings and the bus waveguides is very critical which is challenging when the bend radius is of the order of few micrometers. It seems advantageous if we can select a single wavelength from a single ring resonator without a cascaded ring combinations or reduction in ring radius for specific applications such as chip based tunable lasers[12,13] and multi-analytic label free biosensors.[14,15] This will avoid unwanted spectral interferences and noises in such device to obtain higher side band rejection (SBR) and narrow spectral band width for a single wavelength selection application.

In this context, this paper illustrates a filter configuration which uses a single ring resonator of larger radius connected to a grating resonator at its drop port to achieve single wavelength selection and switching property with high FSR and spectral features suitable for on-chip wavelength selection applications.

II. OPTICAL FILTER DESIGN AND SPECTRAL BEHAVIOUR

A schematic diagram of the proposed filter configuration is shown in Fig. 1(a). It consists of a ring resonator with a grating resonator in its drop port. The waveguide gratings is a vertical side wall gratings on a planar waveguide.[16] The structure parameters of the filter device are shown in Fig. 1(a); where, W is the waveguide width and ΔW is the grating etch depth, n_1, n_2 are the effective refractive indices, and R is the radius of ring resonator.

The grating lengths l_g and l_w are related by the Bragg condition,

$$l_g n_1 + l_w n_2 = \frac{m\lambda_B}{2}, \tag{1}$$

where m is the order of the grating and λ_B is the Bragg wavelength. The resonant cavity is formed by introducing a defect length (phase shift length) of quarter wavelength magnitude,

$$\Lambda p = \frac{\lambda_B}{4n_2} \tag{2}$$

into the gratings at the center. The duty cycle (D) of the gratings is defined by

$$D = \frac{l_w}{\Lambda}. \tag{3}$$

[a]Author to whom correspondence should be addressed. Electronic mail: PPrabhathan@ntu.edu.sg

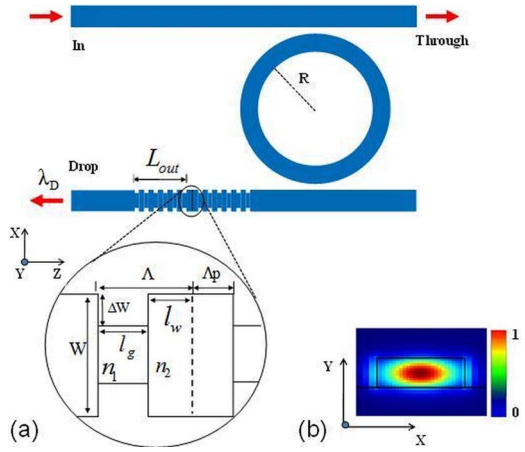

FIG. 1. (a) Schematic diagram of the filter with different structure parameters. (b) Simulated TE mode field intensity at the waveguide cross section.

Assuming a silicon substrate in the simulation, the refractive indices of the core and cladding were set to $n_{Si} = 3.467$ and $n_{Clad} = 1.45$, respectively. The effective refractive indices n_1 and n_2 were calculated as 2.2526 and 2.5398 through a 3D Beam Propagation Method (BPM) mode solver.[17] With these effective index values, the grating period is calculated for a 50% duty cycle ($l_g = l_w$) as

$$\Lambda = l_g + l_w = 323 \text{ nm}. \tag{4}$$

The quarter wave phase shift length is set to

$$\Lambda p = \frac{\lambda_B}{4n_2} = 0.153\ \mu\text{m}, \tag{5}$$

where the Bragg wavelength λ_B is taken as 1.55 μm. The phase shifted gratings can act like a resonator with gratings on both sides as Bragg mirrors. The quantity

$$L_{out} = N\Lambda \tag{6}$$

is the length of the gratings on one side of the central cavity; where, N is the number of grating periods. The ring resonator radius is taken as R = 20 μm with a bus-ring coupling gap of 200 nm. A Silicon-on-Insulator (SOI) strip waveguide with area of cross section of 500 × 250 nm with silica cladding is assumed in the simulation for single mode TE wave propagation. Figure 1(b) shows the simulated electric field intensity distribution for a TE mode in a single mode silicon waveguide. The device simulation is done using Finite Difference Time Domain (FDTD) method.[17] A mesh grid size of 5 nm and time step size of 1.2×10^{-17}s are used in the simulation. The simulation is run for 524 288 (2^{19}) time steps to get a fine spectral resolution of less than 0.3 nm.

Figure 2 shows the spectral response of the filter at the drop and through port. The through port spectrum is similar to a single ring spectral response with equally spaced dropped channels of FSR∼5 nm. The drop port spectrum is characterised by a wide stop band with a single resonant transmission peak at the center. The transmission peak exactly meets at the Bragg wavelength of the grating for a quarter wavelength phase shift at 1.55 μm. Most of the dropped channels are eliminated by the band gap effect of the Bragg gratings, transmitting only a single wavelength at 1.55 μm. The magnified central part (Fig. 2, inset) shows the resonant wavelength has a band rejection (BR) of 26.3 dB at the through-port and drop loss (DL) of < 3 dB at the drop-port. The resonant wavelength has a Side Band Rejection (SBR) of 19.8 dB with channel selectivity (S) ∼ 0.178; where, S is calculated using 1 dB band width $(\Delta\lambda)_{-1\text{ dB}}$ and 3 dB band width $(\Delta\lambda)_{-3\text{ dB}}$ of the resonant wavelength using the equation

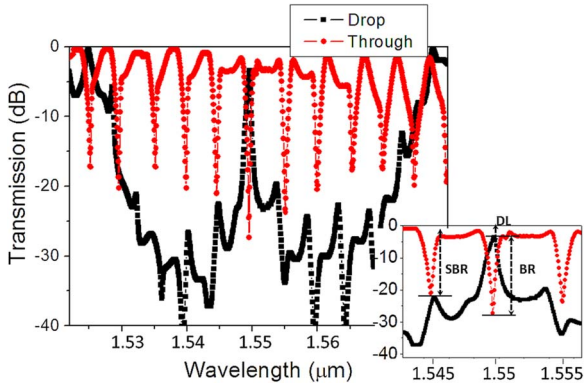

FIG. 2. Transmission spectrum at the drop and through port of the filter Inset shows the magnified resonant transmission at the center.

$$S = \frac{(\Delta\lambda)_{-1\text{ dB}}}{(\Delta\lambda)_{-3\text{ dB}}}. \tag{7}$$

III. Q-FACTOR (Q), RESONANT TRANSMISSION (T), AND LOSS (L) OPTIMISATION IN GRATING RESONATOR

For a wavelength resonant device, a high Q-factor (Q) is very important for low threshold laser applications and a narrow band spectral feature.[18,19] Along with a higher Q value, a higher transmission (T) is also desirable in an optical filter so as to achieve enough power level. For a ring resonator the Q is determined by the surface roughness of the waveguide and bending loss from the ring. This can be controlled through optimized fabrication process and using larger ring radius. For a grating resonator, there are additional design considerations for reducing the scattering loss and mode mismatch loss so that a higher Q can be achieved. Following paragraphs explain how this is achieved in a grating resonator through parameter optimization.

Figure 3(a) shows one of the simulated transmission resonance spectra of a phase shifted gratings with structure parameters Λ = 323 nm, ΔW = 110 nm, and D = 50%. The resonance wavelength is found by fitting a Lorentzian to the transmission peak and Q is obtained by dividing the peak wavelength with its 3 dB bandwidth. The T is defined as normalized power flux at the output that can be detected. For the analysis purpose, the Loss (L) inside the device is defined as part of the power which is not being detected, which is calculated using the following equation

$$L = 1 - (T + R), \tag{8}$$

where R is the reflected power from the grating resonator.

The Q and T is observed to be constant with respect to cavity length variation as shown in Fig. 3(b). With cavity

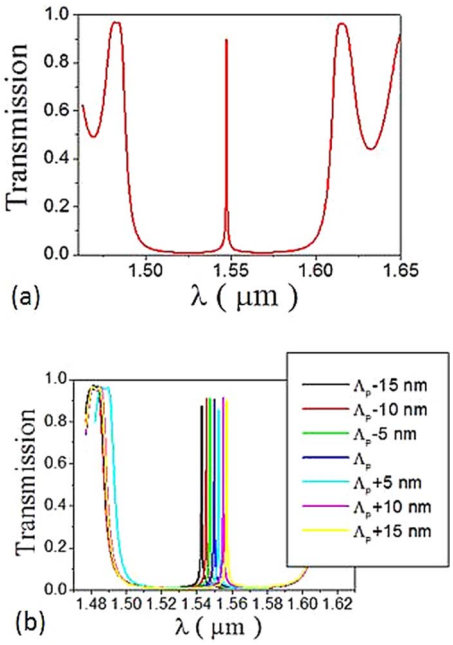

FIG. 3. (a) Normalized transmission spectrum of a phase shifted grating and (b) superposed resonant spectra for varying cavity length.

length variation, the resonant wavelength is observed to be shifting at the rate of 0.52 nm per unit length.

The Bragg mirror reflectivity is a function of grating length, $L_{out} = N\Lambda$, which in turn can be controlled through number of grating periods N. The variation in Q, T, and L with N is plotted in Fig. 4(a). The variation in Q can be divided into two stages. In the first stage Q varies exponentially with respect to N. In the second stage Q varies slowly and reaches to saturation. This behavior in Q can be explained by a Fabry-Perot model of resonant cavity filter. The total Q-factor in a grating resonator is expressed as below:[20]

$$\frac{1}{Q} = \frac{1}{Q_l} + \frac{1}{Q_v}, \tag{9}$$

where Q_l the longitudinal quality factor of the grating resonant cavity which is a function of the longitudinal loss from grating mirrors and depends on the grating coupling coefficient (K) and grating length ($L = N\Lambda$) as

$$Q_l \cong \left(\frac{\pi}{4K\Lambda}\right) \exp(2KL). \tag{10}$$

The term Q_v is the vertical quality factor which is a function of the vertical radiation loss per unit length of the grating (α):

$$Q_v = \left(\frac{\pi}{2\alpha\Lambda}\right). \tag{11}$$

The vertical loss in the structure is mainly due to the out of plane scattering loss and the mode mismatch loss at grating-waveguide interface.

The total Q is limited by Q_l or Q_v depending upon which is the dominant loss mechanism inside the cavity, either longitudinal loss or vertical loss. For a smaller N, longitudinal loss is the dominant loss inside the cavity due to the lower reflectivity of the grating mirror, i.e., $Q_l \ll Q_v$ for smaller N. Hence from Eq. (9), it follows that $Q \approx Q_l$ at smaller N. This corresponds to the region I in Fig. 4(a) as an exponential variation in the Q-factor.

With an increase in N, the longitudinal loss decreases due to the increased grating mirror reflectivity and the vertical loss increases due to the increase in out of plane scattering from more number of grating periods, i.e., $Q_l \gg Q_v$ at higher N. Hence from Eq. (9) it follows that $Q \approx Q_v$ at higher N. This is observed as a linear variation and ultimate saturation in Q for higher N as shown in region II. The exponential to linear behavior in Q factor is due to the increased out of plane scattering loss from increased grating periods at higher N. However, with very high N value the number of grating periods taking part in the reflection process becomes saturated because of lesser light-grating interaction at the outer region of the gratings, which leads to a saturation in the vertical radiation loss. This is observed as the ultimate saturation in the Q-factor.

The T and L variation in region I and region II is explained as below. In the case of transmission, the initial exponential decrease in T with respect to N in region I is due to the exponential increase in grating reflectivity with respect to increase in N. For a higher N, the grating reflectivity saturates and no further increase in grating reflectivity happens. This makes the resonant wavelength tightly bound inside the cavity and the T becomes a constant low value at higher N. The initial gradual increment in L value in region I with increase in N is due to the increase in scattering loss at the grating edges. For a smaller N most of the input light is transmitted through input grating mirror and passes through the second grating mirror due to the lower reflectivity of the gratings, and contribute to the increase in loss. For a higher value in N, a broad spectrum of input light is decoupled from the cavity due to the high reflectivity of the input mirror, eventually leading

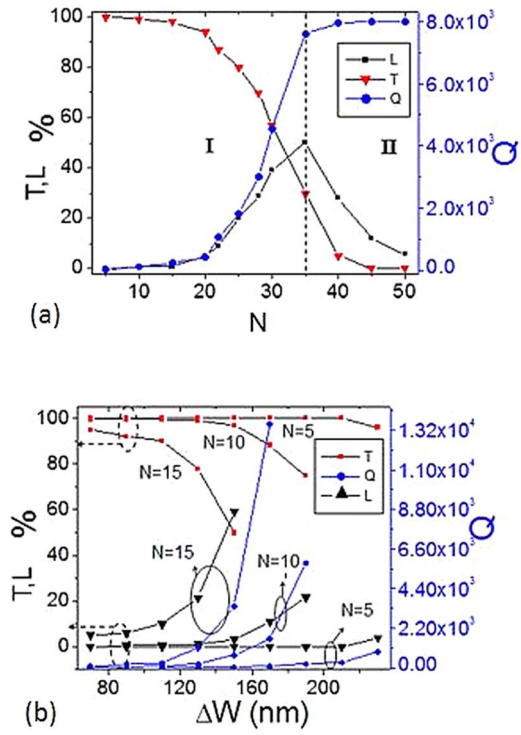

FIG. 4. (a) Variation in Q, T, and L with respect to (a) N and (b) ΔW.

to a narrow band resonant wavelength oscillation inside the cavity. This leads to a reduced loss at higher value of N.

The etch depth ΔW of the grating is another factor which can be controlled in a Bragg mirror. Deeply etched gratings are expected to show strong Bragg reflection. A higher *Q*-value is achieved through highly reflecting grating mirrors through maximizing the index contrast between core and cladding. This is explained by Fig. 4(b) as an exponential increase in *Q* for higher value of ΔW. For a smaller value in grating number (e.g., N = 5), the initial variation is observed to be linear. From the figure it is observed that the gratings with length N = 15 and grating depth of ΔW = 170 nm can give a *Q* of ∼1 × 10^4. A higher length gratings (N = 40) is needed to get the same order *Q* for a grating with ΔW = 110. Whereas, a higher transmission is observed for smaller ΔW. This is due to the lesser out of plane scattering resulting from smaller ΔW.

This type of spectral behavior in these grating resonators suggests that to achieve a higher *Q* along with a higher T there should be a compromise between these two values. The design consideration for a higher *Q* should be an optimum grating number (N) which gives a saturation in *Q* value and then to reduce the loss inside the structure. The out of plane loss inside the structure is reduced by lowering the scattering loss and mode mismatch loss. This is achieved by reducing the filling factor of the gratings. The filling factor which is defined as the percentage of air gap in a period of the grating can be expressed as[21]

$$ff = 2 \cdot \Delta W \cdot (\Lambda - l_w)/(W \cdot \Lambda). \quad (12)$$

A lower *ff* can be achieved through a lower ΔW and a higher D of the gratings. To get a compact design, short gratings length can be chosen (lower N which gives a higher transmission) and then increase ΔW to achieve the required *Q*.

IV. FABRICATION RESULTS

Fabrication of the device was done on a SOI wafer using electron beam lithography using JOEL system. A silicon wafer of 220 nm top silicon layer and 2 μm buried oxide layer was used in the process. A positive tone resist ZEP-520A was used for the electron beam patterning. A resist thickness of 260 nm was used through 4000 RPM, 30 s recipe. An exposure dose of 180 μC/cm^2 and 50 KV voltages was used in the e-beam writing process. The waveguide etching was done using Inductively Coupled Plasma (ICP) Reactive Ion Etching (RIE) machine with Chlorine (Cl_2) and He-O_2 gases at 60 mTorr chamber pressure. In order to get a smooth vertical side wall for the waveguide gratings, a thin layer of SiO_2 hard mask (60 nm thickness) was used in the silicon etching process. Finally, thermal oxidation method was adopted to get a smooth surface profile for the device so that waveguide loss can be reduced. To increase the coupling efficiency between input fibre and the device, the waveguide ends were terminated with Spot Size Converters (SSC) with dimensions 200 μm in length and 180 nm in tip width. A silicon dioxide (SiO_2) cladding layer of 2μm thickness was deposited over the final device through Plasma Enhanced Chemical Vapour Deposition (PECVD) process. Figure 5 shows the Scanning Electron Microscope (SEM) image of one of the fabricated devices before the cladding layer deposition.

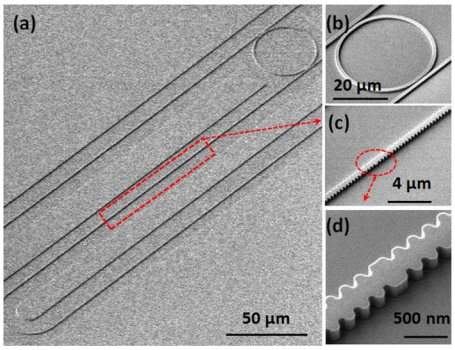

FIG. 5. SEM images of the fabricated device: (a) ring filter with grating resonator at drop port, (b) ring resonator, (c) grating resonator, and (d) gratings with phase shifted region.

Figure 5(a) shows the whole configuration with ring resonator and the waveguide gratings at drop port. Figure 5(b) is the ring resonator having a radius 20 μm. Figure 5(c) shows the grating waveguide and Fig. 5(d) is the magnified gratings showing the phase shifted region. The drop port waveguide was given a semi-circular bend at the output direction for measurement convenience. A series of devices with different grating resonator dimensions are fabricated in the process. This section shows the characterisation results of some of the devices which have a reasonable resonant transmission with a high *Q*-factor.

The device characterisation was done using an Amplified Spontaneous Emission (ASE) light source (EXFO FLS 2300B) and an Optical Spectrum Analyser (AQ6317B). Two lensed polarisation maintaining fibres were used to couple light in and out of the silicon waveguide. A polarisation controller (PC) was used to select TE mode (electric field parallel to the substrate plane) from the ASE source. Precise in- and out- coupling was achieved through 3-axis micro positioning stages aligned by a motor controller. The through port spectral response shows equally spaced extinction channels with FSR ∼5.2 nm (see Fig. 6). This is a typical drop port spectral response of a single ring resonator with radius 20 μm. The drop-port spectral responses of the filter configuration for the four different grating resonator dimensions are shown in Fig. 7. The respective phase shifted grating dimensions are

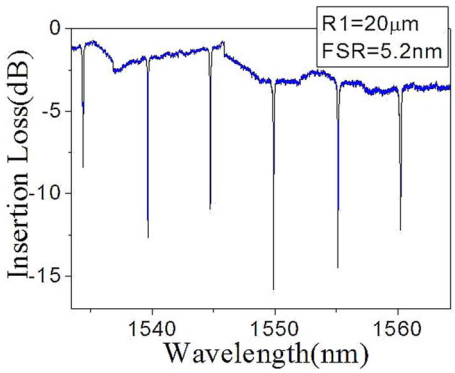

FIG. 6. Through- port spectrum from the filter.

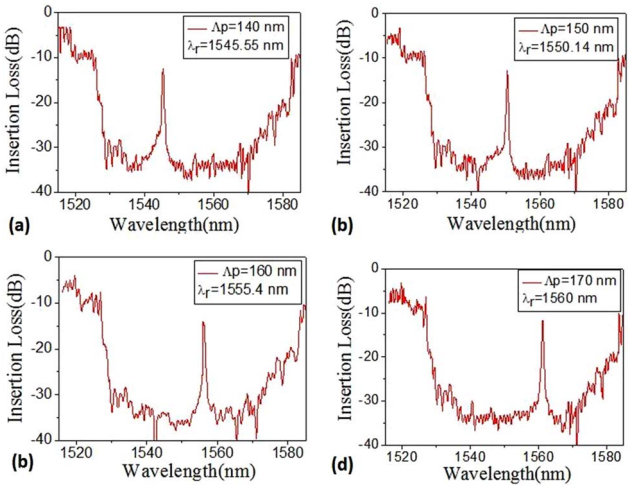

FIG. 7. Drop-port filter spectra with different phase shifted gratings dimensions: (a) $\Lambda p = 140$ nm, (b) $\Lambda p = 150$ nm, (c) $\Lambda p = 160$ nm, and (d) $\Lambda p = 170$ nm.

140 nm, 150 nm, 160 nm, and 170 nm, with gratings features kept same for all, viz., W = 500 nm, $\Lambda = 323$ nm, $\Delta W = 120$ nm, D = 60%, and N = 30. A single resonance peak is observed at the centre of a wide stop band (∼60 nm) with a 3-dB resonance band width of ∼ 0.4 nm and an out of band rejection ratio > 15 dB. The *Q*-factor of the resonance is calculated as $\sim 4 \times 10^3$. This value is in close resemblance to the value observed in the simulation for the gratings specifications used. The spectral response for the filter has shown resonant wavelength switching characteristics with respect to the variation in phase shifted dimension. Resonant wavelength switching to adjacent drop port spectrum is observed through the cavity length variation. The quarter wavelength dimension 140 nm, 150 nm, 160 nm, and 170 nm shows resonant wavelengths at 1545.55 nm, 1550.14 nm, 1555.4 nm, and 1560 nm, respectively.

V. CONCLUSION

A wavelength filter configuration has been demonstrated using a ring resonator and grating resonator combination to achieve single wavelength selection and switching property suitable for on-chip wavelength selection applications. The proposed configuration is expected to find applications in silicon photonics devices such as, on-chip external cavity lasers, and multi analytic label-free biosensors. The grating resonator has been designed for a high *Q*-factor, high transmittivity, and minimum loss so that the wavelength selectivity of the device is improved. The proof-of-concept device has been demonstrated on a Silicon-on-Insulator (SOI) platform through electron beam lithography and Reactive Ion Etching (RIE) process. The transmission spectrum shows narrow band single wavelength selection and switching property with a high Free Spectral Range (FSR) ∼60 nm and side band rejection ratio >15 dB.

ACKNOWLEDGMENTS

The authors acknowledge the COLE-EDB funding and MOE–AcRF Tier 1 funding for the financial support towards the project.

[1]R. Soref, *Silicon Photonics: The State of the Art*, edited by G. T. Reed (John Wiley & Sons, Ltd., 2008).
[2]P. Orlandi, C. Ferrari, M. J. Strain, A. Canciamilla, F. Morichetti, M. Sorel, P. Bassi, and A. Melloni, Opt. Lett. **37**, 3669 (2012).
[3]K. A. Rutkowska, D. Duchesne, M. J. Strain, R. Morandotti, M. Sorel, and J. Azaña, Opt. Express **19**, 19514 (2011).
[4]L. Eldada, Rev. Sci. Instrum. **75**, 575 (2004).
[5]K. De Vos, I. Bartolozzi, E. Schacht, P. Bienstman, and R. Baets, Opt. Express **15**, 7610 (2007).
[6]A. Densmore, M. Vachon, D. X. Xu, S. Janz, R. Ma, Y. H. Li, G. Lopinski, A. Delâge, J. Lapointe, C. C. Luebbert, Q. Y. Liu, P. Cheben, and J. H. Schmid, Opt. Lett. **34**, 3598 (2009).
[7]P. Prabhathan, V. M. Murukeshan, Z. Jing, and P. V. Ramana, Opt. Express **17**, 15330 (2009).
[8]P. Prabhathan, V. M. Murukeshan, and J. Zhang, Opt. Eng. **51**, 044604 (2012).
[9]Q. Xu, D. Fattal, and R. G. Beausol, Opt. Express **16**, 4309 (2008).
[10]Y. Yanagase, S. Suzuki, Y. Kokubun, and S. T. Chu, J. Lightwave Technol. **20**, 1525 (2002).
[11]P. Prabhathan, J. Zhang, V. M. Murukeshan, H. Zhang, and S. Chen, IEEE Photonics Technol. Lett. **24**, 152 (2012).
[12]N. Keita, K. Tomohiro, and Y. Hirohito, Appl. Phys. Express **5**, 082701 (2012).
[13]K. Tomohiro, N. Keita, and Y. Hirohito, Jpn. J. Appl. Phys. **53**, 04EG04 (2014).
[14]D. Dai, Opt. Express **17**, 23817 (2009).
[15]S. Mandal and D. Erickson, Opt. Express **16**, 1623 (2008).
[16]P. Prabhathan, V. M. Murukeshan, Zhang Jing, and P. V. Ramana, Appl. Opt. **48**, 5598 (2009).
[17]OptiFDTD-7, Optiwave Corporation, Ottawa, ON, Canada.
[18]O. Painter, R. K. Lee, A. Scherer, A. Yariv, J. D. O'Brien, P. D. Dapkus, and I. Kim, Science **284**, 1819 (1999).
[19]A. R. Md Zain, N. P. Johnson, M. Sorel, and R. M. De La Rue, Opt. Express **16**, 12084 (2008).
[20]H. A. Haus, *Waves and Fields in Optoelectronics* (Prentice Hall, Englewood cliffs, NJ, 1984).
[21]M. Gnan, G. Bellanca, H. M. H. Chong, P. Bassi, and R. M. De La Rue, Opt. Quantum Electron. **38**, 133 (2006).